



# Molecular beam epitaxy of superconducting zirconium nitride on GaN substrates

December 2024

*Changing the World's Energy Future*

Brelon James May, Sabin Regmi, Amey Rajendra Khanolkar, Volodymyr Borysovyh Buturlim, Zachery Earl Cresswell, Kevin Daniel Vallejo, Krzysztof Gofryk, David H Hurley



**DISCLAIMER**

This information was prepared as an account of work sponsored by an agency of the U.S. Government. Neither the U.S. Government nor any agency thereof, nor any of their employees, makes any warranty, expressed or implied, or assumes any legal liability or responsibility for the accuracy, completeness, or usefulness, of any information, apparatus, product, or process disclosed, or represents that its use would not infringe privately owned rights. References herein to any specific commercial product, process, or service by trade name, trade mark, manufacturer, or otherwise, does not necessarily constitute or imply its endorsement, recommendation, or favoring by the U.S. Government or any agency thereof. The views and opinions of authors expressed herein do not necessarily state or reflect those of the U.S. Government or any agency thereof.

# **Molecular beam epitaxy of superconducting zirconium nitride on GaN substrates**

**Brelon James May, Sabin Regmi, Amey Rajendra Khanolkar, Volodymyr Borysovych Buturlim, Zachery Earl Cresswell, Kevin Daniel Vallejo, Krzysztof Gofryk, David H Hurley**

**December 2024**

**Idaho National Laboratory  
Idaho Falls, Idaho 83415**

**<http://www.inl.gov>**

**Prepared for the  
U.S. Department of Energy  
Under DOE Idaho Operations Office  
Contract DE-AC07-05ID14517, DE-AC07-05ID14517**

RESEARCH ARTICLE | DECEMBER 24 2024

# Molecular beam epitaxy of superconducting zirconium nitride on GaN substrates <sup>EP</sup>

Brelon J. May ; Sabin Regmi ; Amey R. Khanolkar ; Volodymyr Buturlim ; Zachery E. Cresswell ; Kevin D. Vallejo ; Krzysztof Gofryk ; David H. Hurley 



AIP Advances 14, 125327 (2024)

<https://doi.org/10.1063/5.0242982>



View  
Online



Export  
Citation

## Articles You May Be Interested In

Pressure-induced kinetics of the  $\alpha$  to  $\omega$  transition in zirconium

*J. Appl. Phys.* (July 2015)

Atomic layer deposition of hafnium and zirconium oxyfluoride thin films

*J. Vac. Sci. Technol. A* (January 2021)

*In situ* stress measurements in zirconium and zirconium oxide films prepared by direct current sputtering

*J. Appl. Phys.* (June 2006)

## AIP Advances

### Why Publish With Us?



**19 DAYS**  
average time  
to 1st decision



**500+ VIEWS**  
per article (average)



**INCLUSIVE**  
scope

[Learn More](#)

# Molecular beam epitaxy of superconducting zirconium nitride on GaN substrates

Cite as: AIP Advances 14, 125327 (2024); doi: 10.1063/5.0242982

Submitted: 11 October 2024 • Accepted: 6 December 2024 •

Published Online: 24 December 2024











View Online



Export Citation



CrossMark

Brelon J. May,<sup>a)</sup>  Sabin Regmi,  Amey R. Khanolkar,  Volodymyr Buturlim,  Zachery E. Cresswell,   
Kevin D. Vallejo,  Krzysztof Gofryk,  and David H. Hurley 

## AFFILIATIONS

Idaho National Laboratory, Idaho Falls, Idaho 83415, USA

<sup>a)</sup> Author to whom correspondence should be addressed: [brelon.may@inl.gov](mailto:brelon.may@inl.gov)

## ABSTRACT

Epitaxial integration of metals and semiconductors can enable enhanced performance and novel functionality. Achieving such pristine interfaces with superconducting materials is of increasing interest for quantum devices and detectors, but the experimental demonstration remains challenging, given the very limited studies on single crystalline systems. To expand the potential materials for these systems, this work explores the deposition of zirconium nitride superconducting thin films on GaN substrates at various temperatures using molecular beam epitaxy. A general trend of decreasing superconducting critical temperature is observed as the deposition temperature is reduced. The optical properties reveal a transition from metallic to dielectric behavior with colder deposition. The plasma frequency of the metallic films is also observed to be a function of growth temperature. These results pave the way for the integration of a highly tunable metal nitride with a well-established semiconductor system.

© 2024 Author(s). All article content, except where otherwise noted, is licensed under a Creative Commons Attribution-NonCommercial 4.0 International (CC BY-NC) license (<https://creativecommons.org/licenses/by-nc/4.0/>). <https://doi.org/10.1063/5.0242982>

Interfaces between materials are of utmost importance in modern electronic device architectures. However, when it comes to integrating metals and semiconductors, the interface is often overlooked despite the advantages of epitaxial interfaces such as enhanced conductivity and transit time.<sup>1,2</sup> Such interfaces could enable hyperbolic metamaterials,<sup>3</sup> metallic contacts with tailored work functions,<sup>4,5</sup> and novel device architectures.<sup>6</sup> The incompatibility between the two classes of materials due to differences in bonding, symmetry, lattice parameter, and growth conditions makes epitaxial integration difficult. The list of metal–semiconductor systems which have been successfully demonstrated is relatively small,<sup>7,8</sup> and the list of superconducting metals is even smaller.

The epitaxial integration of superconductors and semiconductors could result in improved performance of Josephson junction qubits, Josephson junction lasers, and single photon detectors and enable new topological electron systems.<sup>9–14</sup> The wurtzite (InGaAl)N material system allows for a wide tunability of bandgap ranging from infrared to deep ultraviolet and high breakdown voltages and is the backbone of the blue LED and power electronics industry. Transition metal nitrides (TMNs) have a range of attractive properties spanning from high temperatures and chemical stability

to high hardness and can host various forms of magnetism.<sup>15–18</sup> In addition, a number of them are superconducting at low temperatures<sup>19</sup> and have also been reported to have strain-tunable superconducting critical temperatures ( $T_c$ ).<sup>20,21</sup> Select hexagonal ( $\delta'$ -NbN,  $\beta$ -Nb<sub>2</sub>N, and  $\gamma$ -Ta<sub>2</sub>N) and cubic TMNs (TiN,  $\delta$ -NbN, TaN, and GdN) have been demonstrated on III-N or 6H-SiC substrates and even fabricated into devices with exciting properties.<sup>14,22–25</sup> The hexagonal and cubic polytypes of TMNs deposited on c-plane substrates grow along the [0001] and [111] directions, respectively. GaN substrates are closely lattice matched to cubic rock salt NbN (+1.4%) and TaN (+2.0%) when comparing the cubic [110] to the [1 $\bar{1}$ 20] direction of the hexagonal materials.

ZrN is another rock salt structured TMN with a lattice mismatch to GaN of only –0.5%. The mechanical properties of ZrN have been well-studied,<sup>26,27</sup> and it is an ohmic contact to n-type GaN<sup>28</sup> and is a known superconductor with a critical temperature of 10 K and a critical field of 6.40 T.<sup>29</sup> Most studies on thin films of this material have been polycrystalline material synthesized using pulsed laser deposition or sputtering.<sup>30</sup> However, while there are limited reports of chemical vapor deposition of GaN on sputtered epitaxial ZrN films,<sup>31</sup> there have been no reports of deposition of this material

via molecular beam epitaxy (MBE) or its growth on GaN. This paper discusses the MBE growth of ZrN on GaN at several different substrate temperatures. Since it is known that off-stoichiometries are prevalent in the Ta and Nb nitrides deposited using MBE,<sup>23,24,32,33</sup> we will henceforth refer to the thin films deposited here as Zr<sub>x</sub>N<sub>y</sub>.

Thin films were deposited on c-plane GaN/Al<sub>2</sub>O<sub>3</sub> templates at various temperatures using a Veeco GENxplor system. A multi-temperature substrate holder (III-V components) was used to simultaneously hold substrates at different temperatures during simultaneous deposition.<sup>34</sup> More details on this setup are provided in the [supplementary material](#). The substrate was rotated continuously during deposition, and the temperature of each substrate was continuously monitored using a k-Space Associates BandiT in black-body mode. All samples were simultaneously exposed to nitrogen plasma when the hottest sample on the MTZ holder reached 500 °C to prevent decomposition of the GaN surface. Nitrogen was supplied using a Veeco plasma source operated at 300 W and a flow rate of 3 SCCM; corresponding to a N flux of  $1 \times 10^{15}$  atoms/cm<sup>2</sup> s calibrated using RHEED transients of metal-rich GaN homoepitaxy at 750 °C. The Zr was supplied via heating 4 N pure pellets in a carbon crucible and heated using a Telemark electron beam at an output power correlating to a nominal growth rate of 2.4 nm/min (a flux of  $1.66 \times 10^{14}$  atoms/cm<sup>2</sup> s). Once the substrate temperatures ( $T_{\text{sub}}$ ) reached the desired range, the samples were all exposed to Zr and N for 25 min. The samples were then cooled under exposure to the nitrogen plasma until the hottest sample was <500 °C. The influence of the substrate temperature on the crystal structure, resistivity, and optical properties was investigated. X-ray diffraction (XRD) measurements were taken on a Bruker D8 Advance x-ray diffractometer, 4-point resistivity measurements were taken as a function of temperature down to 2.5 K on a Quantum Design physical property measurement system (PPMS), and ellipsometry measurements were taken on a J.A. Woollam M-2000 ellipsometer with an Auto Angle ESM-300 Base at room temperature.

**Figure 1** shows the XRD for Zr<sub>x</sub>N<sub>y</sub> deposited at  $T_{\text{sub}}$  from 530 to 970 °C. The substrate peaks are marked with asterisks and include those that appear at  $\sim 52^\circ$ , which are due to the Renninger effect, which results in diffraction of normally forbidden odd-order peaks in c-plane GaN.<sup>35</sup> The primary diffraction peaks at all temperatures are close to the GaN substrate peaks. At growth temperatures

>738 °C, a clear peak emerges at  $\sim 40^\circ$  corresponding to the (001) orientation of a matching cubic Zr<sub>x</sub>N<sub>y</sub> phase that showed a (111) peak at the lower angle and is marked with a square. Thus, we postulate that all the primary peaks are due to the same phase and the underlying substrate is forcing the material to grow (111) oriented, despite the formation of (001) being more favorable at elevated temperatures. The Zr<sub>x</sub>N<sub>y</sub> (001) peaks are most intense at  $T_{\text{sub}} = 810^\circ\text{C}$  (yellow); this is also the only temperature at which the peaks near to the substrate decrease in intensity, suggesting a possible existence of a growth window for a (001)-oriented Zr<sub>x</sub>N<sub>y</sub>.

A closer look at the second order reflections [**Fig. 1(b)**] reveals that increasing  $T_{\text{sub}}$  results in the diffraction peak shifting to lower angles, increasing in intensity, and decreasing full-width at half maximum. There are several potential stable or metastable cubic and hexagonal Zr<sub>x</sub>N<sub>y</sub> phases, which have (111) or (0001) planes, marked with triangles, which would also give strong diffraction in the 70–72° range.<sup>36</sup> The lower intensity and peak shift with decreasing  $T_{\text{sub}}$  could correspond to a transition to an amorphous Zr<sub>3</sub>N<sub>4</sub> phase.<sup>37</sup> The extracted parameters from peak fitting are plotted in **Fig. 1(c)**. This peak fitting (details in the [supplementary material](#)) reveals that the high angle shoulders, which are observed in all samples, correspond to diffraction emerging from the Cu  $\kappa\alpha_2$  x rays. However, the shoulder in the sample with  $T_{\text{sub}} = 810^\circ\text{C}$  cannot be fully explained by Cu  $\kappa\alpha_2$  and shows the presence of peaks at 71.24 and 71.44°. This sample also has the largest parasitic (001) peak at 41°, which could signify the growth of competing phases with similar lattice constants under these conditions. RHEED at different rotations, on similar samples (**Fig. S2.1** of the [supplementary material](#)), reveals that an azimuthal relationship is maintained between the deposited Zr<sub>x</sub>N<sub>y</sub> and the underlying GaN substrate, signifying some epitaxial relationship.

The electrical resistivity ( $\rho$ ) of Zr<sub>x</sub>N<sub>y</sub> films was measured as a function of temperature and magnetic field. The resistivity of the samples varies over orders of magnitude; thus, the  $\rho$  normalized to the resistivity at 250 K [**Fig. 2(a)**] and 11 K [**Fig. 2(b)**] is plotted to allow for easier observation of the trends and features, and the extracted parameters from these data are displayed in **Fig. 2(c)**. The transport properties of these samples generally follow trends indicative of metallic behavior. The sample deposited at 884 °C shows the lowest  $\rho$  at both elevated temperature and low temperature,

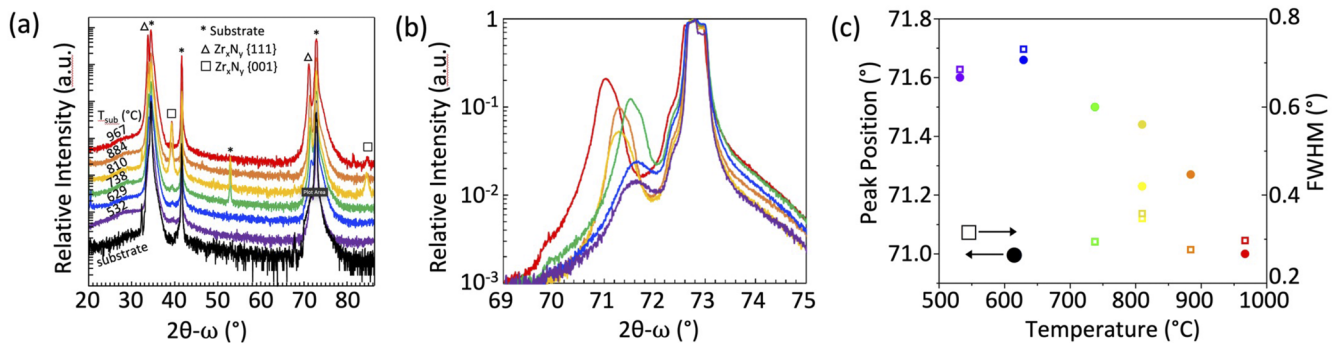


**FIG. 1.**  $2\theta$ - $\omega$  XRD diffraction patterns for Zr<sub>x</sub>N<sub>y</sub> over (a) a wide angle and (b) magnified about the second order reflections. (c) Extracted peak positions of the second order peaks.

16.5 ( $T = 16.5$  K) and  $6.7 \mu\Omega\text{-cm}$  ( $T = 10$  K), respectively. The room temperature  $\rho$  for this sample is  $19 \mu\Omega\text{-cm}$ , close to the value observed for bulk rock salt ZrN ( $12 \mu\Omega\text{-cm}$ ), and within the range of observed resistivity for films made by other methods.<sup>38,39</sup> This sample also had the highest residual resistivity ratio (RRR), defined for these samples as  $\rho(250 \text{ K})/\rho(11 \text{ K})$ . Deviation from  $T_{\text{sub}} = 884^\circ\text{C}$  results in higher resistivities and a lower RRR. The sample deposited at the lowest  $T_{\text{sub}}$  has an RRR of  $\sim 1$ . This contrasts what is displayed in Fig. 2(a), where  $\rho/\rho(250 \text{ K}) > 1$ . Normalization with respect to  $\rho(250 \text{ K})$  was done because of an observed sharp drop in  $\rho$  observed at  $\sim 290$  K for this sample (supplementary material). After this drop, the  $\rho$  continues to decrease in a metallic fashion until  $\sim 80$  K when  $\rho$  increases, before starting to turn down at  $\sim 3.2$  K. Detailed investigation into the atypical temperature dependent resistivity in this sample is beyond the scope of the current investigation.

The superconducting critical temperatures ( $T_c$ ) are defined as the position of the maximum in the first derivative  $\delta\rho/\delta T$ , and  $T_{\rho=0}$  is defined by the first data point at which  $\rho \approx 0$ . Decreasing  $T_{\text{sub}}$  shows a general decrease in the observed  $T_c$  values [Fig. 2(c3)]. The sample with the highest  $T_{\text{sub}}$  shows the first sharp drop in  $\rho$  at  $T_{c1} = 8.5$  K. However, despite another drop at  $T_{c2} = 7.1$  K, the resistance does not drop to zero for this sample. These features suggest the presence of discrete regions of off-stoichiometry or phases that have different  $T_c$  values.<sup>40</sup> When there is no percolation path between these regions, plateaus arise in the resistivity until the temperature is decreased below the critical temperature of other regions and a lossless conduction path is formed. While the  $T_c$  values generally trend toward

lower temperatures as  $T_{\text{sub}}$  decreases, the presence of a complete percolation path does not follow the same trend. However, there seem to be shared values in which the temperature drops occur, suggesting that it is not a smooth variation in  $T_c$ , and rather the coexistence of discrete phases or off-stoichiometries, which are more stable in these samples. The XRD shown previously does not suggest the presence of a large amount of another phase for any sample other than  $T_{\text{sub}} = 810^\circ\text{C}$ . Interestingly, this sample also falls most out of the resistance trends observed, showing a gradual drop that is estimated to have a  $T_c$  of  $\sim 3.9$  K, but does not drop to zero in the temperature range measured. The magnetoresistance reveals that samples with similar critical temperatures also share similar critical fields suggesting the presence of shared phases. More details regarding magnetoresistance are provided in the supplementary material.

The as-grown samples for high  $T_{\text{sub}}$  were an opaque silver-gold, but as  $T_{\text{sub}}$  decreased, this transitioned to a translucent purple for the lowest growth temperature. Thus, room temperature ellipsometry was performed to investigate the optical properties and correlate with the transport behavior. Figure 3 shows the permittivity in real and imaginary space ( $\epsilon'$  and  $\epsilon''$ ), refractive index ( $n$ ), and extinction coefficient ( $k$ ). The fitting details are supplied in the supplementary material. The samples show a divided behavior; the high temperature samples ( $T_{\text{sub}} > 800^\circ\text{C}$ ) and the low temperature samples ( $T_{\text{sub}} < 700^\circ\text{C}$ ) are grouped together, while the sample with  $T_{\text{sub}} = 738^\circ\text{C}$  lies between the two types.

Across the wavelengths measured,  $\epsilon'$  is positive for low  $T_{\text{sub}}$  samples signifying more dielectric-like materials, but high values

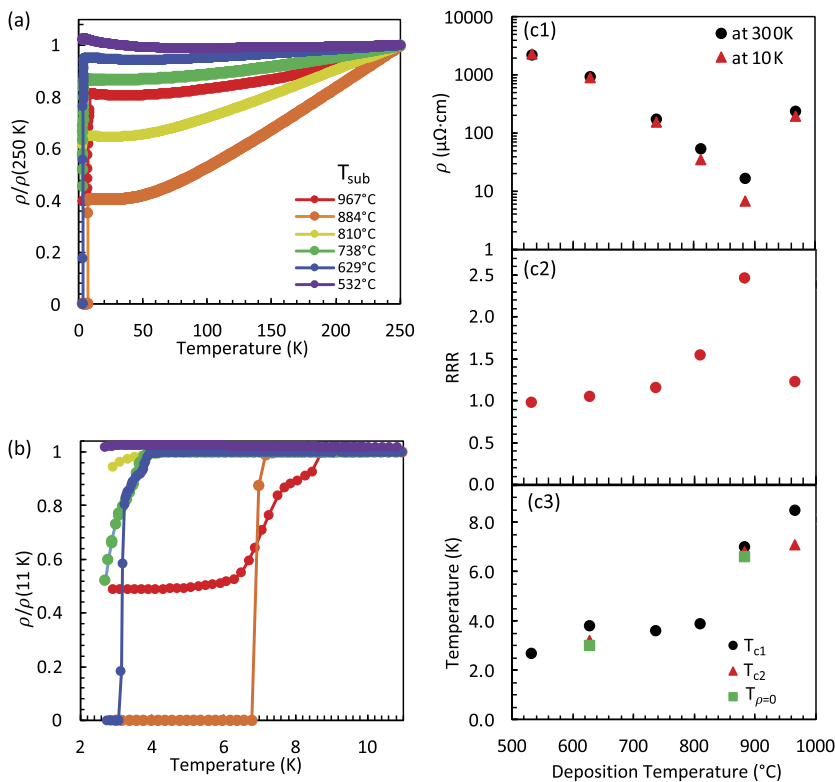


**FIG. 2.** (a) Resistivity normalized to the value at 250 K for samples deposited at different  $T_{\text{sub}}$ . (b) Magnification of the low temperature region normalized to  $\rho(11 \text{ K})$ . (c) Extracted parameters showing (c1)  $\rho$  at 250 K (black) and 10 K (red), (c2) RRR, and (c3) temperatures where drops in  $\rho$  are observed.



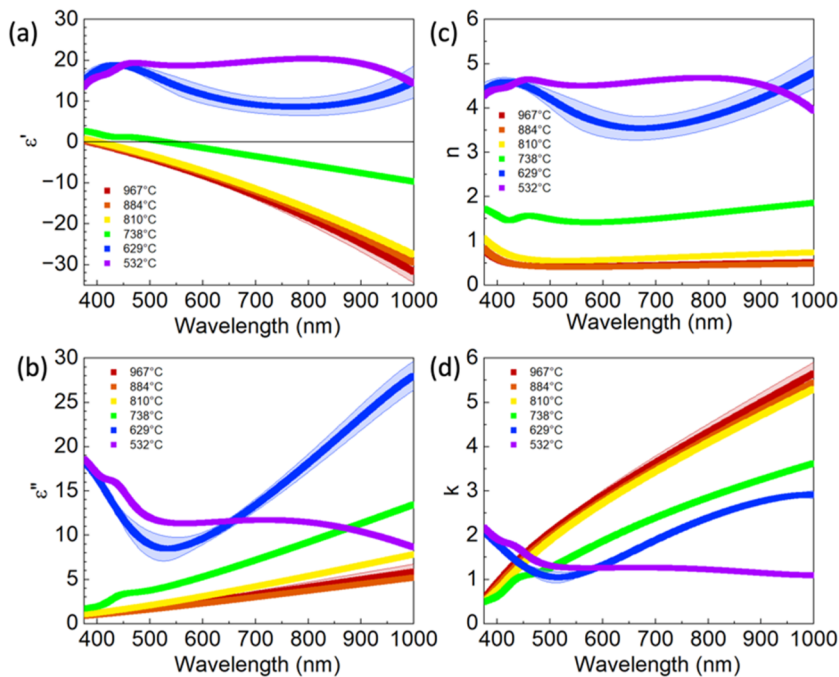


**FIG. 3.** Values of (a)  $\epsilon'$ , (b)  $\epsilon''$ , (c)  $n$ , and (d)  $k$ , calculated from ellipsometry on samples grown at various  $T_{\text{sub}}$ . The shaded regions represent error bars from measurements conducted at multiple locations on the substrate. If not visible, they lie within the width of the data points.

for  $\epsilon''$  would mean they were also lossy. This matches the electrical transport for the lowest temperature sample. Samples with  $T_{\text{sub}} \geq 738^\circ\text{C}$  have largely negative  $\epsilon'$  over the wavelengths measured, but the wavelength they cross over zero increases with decreasing temperature from 388, 402 to 534 nm. This corresponds to a change in the plasma frequency of the material. The imaginary part ( $\epsilon''$ ) is positive for all samples at these wavelengths, but the high temperature samples begin to approach zero at short wavelengths. The complex permittivity shows a distinct difference, especially at short wavelengths, between the high and low temperature samples. The quality factor of a plasmonic material can be defined as  $Q = \epsilon'/\epsilon''$ ,<sup>41,42</sup> and while the absolute value of  $Q$  is not as high for these materials, as say Ag or Au, it is still increasing at long wavelengths, so the high  $T_{\text{sub}}$  materials could be useful for long-wave applications.

The refractive indices are also broken into similar groups. The low  $T_{\text{sub}}$  samples show higher values and a more wavelength dependence than the high  $T_{\text{sub}}$  samples. With decreasing  $T_{\text{sub}}$ ,  $k$  generally decreases. This holds true at long wavelengths, but there is an inflection at  $\sim 500$  nm for the low  $T_{\text{sub}}$  samples, which begin to absorb more strongly than the high  $T_{\text{sub}}$  samples  $< 450$  nm. Reports on  $\text{Zr}_x\text{N}_y$  films deposited via other methods show similar tunability in optical properties by changing other growth parameters such as N overpressure, flow rate, or oxygen concentration, indicating a strong dependence on stoichiometry.<sup>43</sup> These general trends of these optical properties agree with the structural and electronic transport property measurements discussed earlier in this paper. This work showed the changes in  $\text{Zr}_x\text{N}_y$  properties as a function of temperature when deposited by MBE. The similarity in the position and symmetry of peaks observed in RHEED suggests a high degree of crystallinity and azimuthal orientation with respect to the substrate. While samples deposited at elevated temperatures appear highly

crystalline, XRD shifts at lower temperatures suggest a variation in stoichiometry and loss of crystallinity. The shift in diffraction peaks correlates with different superconducting critical temperatures ranging from 3.2 to 8.8 K, with higher deposition temperatures showing generally higher  $T_c$  values. However, the highest temperature sample did not show the lowest resistivity. Temperature dependent resistivity measurements showed that decreasing the growth temperature results in increased resistivity, eventually transitioning to a more insulator-like behavior. This was supported by room temperature ellipsometry where the low and high growth temperatures were more dielectric and metallic, respectively. In addition, a growth temperature dependence of the plasma wavelength of the metallic samples was also observed. This work opens the door for the integration of another superconducting and plasmonic transition metal nitride with wide bandgap semiconductors using MBE.

## SUPPLEMENTARY MATERIAL

See the [supplementary material](#) for information on the following: (1) multi-temperature zone growth methods, (2) RHEED images of  $\text{Zr}_x\text{N}_y$  films on GaN templates, (3) details on XRD peak deconvolution and relationships with resistivity data, and (4) optical property characterization using spectroscopic ellipsometry.

## ACKNOWLEDGMENTS

The authors acknowledge their funding support. B.J.M., K.D.V., K.G., and V.B. acknowledge the support from Idaho National Laboratory's Laboratory Directed Research and Development (LDRD) program under DOE Idaho Operations Office



Contract No. DE-AC07-05ID14517. A.R.K., D.H.H., and S.R. were supported by the Center for Thermal Energy Transport under Irradiation (TETI), an Energy Frontier Research Center funded by the U.S. Department of Energy, Office of Science, Office of Basic Energy Sciences. Z.E.C. acknowledges the support of the Department of Energy Minority Serving Institution Partnership Program (MSIPP) managed by the Savannah River National Laboratory under BSR.

## AUTHOR DECLARATIONS

### Conflict of Interest

The authors have no conflicts to disclose.

### Author Contributions

**Brelon J. May:** Conceptualization (equal); Data curation (equal); Formal analysis (equal); Funding acquisition (equal); Investigation (equal); Methodology (equal); Supervision (equal); Writing – original draft (equal); Writing – review & editing (equal). **Sabin Regmi:** Data curation (equal); Formal analysis (equal); Investigation (equal); Writing – review & editing (equal). **Amey R. Khanolkar:** Data curation (equal); Formal analysis (equal); Investigation (equal); Writing – original draft (equal); Writing – review & editing (equal). **Volodymyr Buturlim:** Data curation (equal); Formal analysis (equal); Writing – review & editing (equal). **Zachery E. Cresswell:** Data curation (equal); Investigation (equal); Writing – review & editing (equal). **Kevin D. Vallejo:** Investigation (equal); Writing – review & editing (equal). **Krzysztof Gofryk:** Funding acquisition (equal); Investigation (equal); Methodology (equal); Writing – review & editing (equal). **David H. Hurley:** Funding acquisition (equal); Writing – review & editing (equal).

### DATA AVAILABILITY

The data that support the findings of this study are available from the corresponding author upon reasonable request.

### REFERENCES

- S. M. Sze and H. K. Gummel, *Solid-State Electron.* **9**(8), 751–769 (1966).
- D. P. Kumah, J. H. Ngai, and L. Kornblum, *Adv. Funct. Mater.* **30**(18), 1901597 (2020).
- B. Saha, G. V. Naik, S. Saber, C. Akatay, E. A. Stach, V. M. Shalaev, A. Boltasseva, and T. D. Sands, *Phys. Rev. B* **90**(12), 125420 (2014).
- P. Schindler, E. R. Antoniuk, G. Cheon, Y. Zhu, and E. J. Reed, [arXiv:2011.10905](https://arxiv.org/abs/2011.10905) (2020).
- U. W. Pohl, *Epitaxy of Semiconductors* (Springer, 2020).
- D. Jena, R. Page, J. Casamento, P. Dang, J. Singhal, Z. Zhang, J. Wright, G. Khalsa, Y. Cho, and H. G. Xing, *Jpn. J. Appl. Phys.* **58**(SC), SC0801 (2019).
- T. Sands, C. J. Palmström, J. P. Harbison, V. G. Keramidis, N. Tabatabaie, T. L. Cheeks, R. Ramesh, and Y. Silberberg, *Mater. Sci. Rep.* **5**(3), 99–170 (1990).
- B. Saha, A. Shakouri, and T. D. Sands, *Appl. Phys. Rev.* **5**(2), 021101 (2018).
- K. Makise, R. Sun, H. Terai, and Z. Wang, *IEEE Trans. Appl. Supercond.* **25**(3), 1–4 (2015).
- M. Kjærgaard, H. J. Suominen, M. Nowak, A. Akhmerov, J. Shabani, C. Palmström, F. Nichele, and C. M. Marcus, *Phys. Rev. Appl.* **7**(3), 034029 (2017).
- B. H. Elfeky, N. Lotfizadeh, W. F. Schiela, W. M. Strickland, M. Dartiaillh, K. Sardashti, M. Hatefipour, P. Yu, N. Pankratova, H. Lee *et al.*, *Nano Lett.* **21**(19), 8274–8280 (2021).
- M. Cassidy, A. Bruno, S. Rubbert, M. Irfan, J. Kammhuber, R. Schouten, A. Akhmerov, and L. Kouwenhoven, *Science* **355**(6328), 939–942 (2017).
- A. Iovan, A. Pedecheș, T. Descamps, H. Rotella, I. Florea, F. Semond, and V. Zwiller, *Appl. Phys. Lett.* **123**(25), 252602 (2023).
- P. Dang, G. Khalsa, C. S. Chang, D. S. Katzer, N. Nepal, B. P. Downey, V. D. Wheeler, A. Suslov, A. Xie, E. Beam *et al.*, *Sci. Adv.* **7**(8), eabf1388 (2021).
- B. Navinsek and S. Seal, *JOM* **53**, 51–54 (2001).
- C. Hu, K. Guo, Y. Li, Z. Gu, J. Quan, S. Zhang, and W. Zheng, *Thin Solid Films* **688**, 137339 (2019).
- W. R. Lambrecht, M. Miao, and P. Lukashev, *J. Appl. Phys.* **97**(10), 10D306 (2005).
- K. Ito, S. Honda, and T. Suemasu, *Nanotechnology* **33**(6), 062001 (2021).
- Z.-W. Liao, X.-W. Yi, J.-Y. You, B. Gu, and G. Su, *Phys. Rev. B* **108**(1), 014501 (2023).
- W. Lu, H. Zhai, Q. Li, and C. Chen, *J. Phys. Chem. Lett.* **12**(7), 1985–1990 (2021).
- Y. Zou, Q. Jin, Y. Wang, K. Jiang, S. Wang, Y. Li, E.-J. Guo, and Z. G. Cheng, *Phys. Rev. B* **105**(22), 224516 (2022).
- R. Yan, G. Khalsa, S. Vishwanath, Y. Han, J. Wright, S. Rouvimov, D. S. Katzer, N. Nepal, B. P. Downey, D. A. Muller, H. G. Xing, D. J. Meyer, and D. Jena, *Nature* **555**(7695), 183–189 (2018).
- D. S. Katzer, N. Nepal, M. T. Hardy, B. P. Downey, D. F. Storm, E. N. Jin, R. Yan, G. Khalsa, J. Wright, A. C. Lang, T. A. Growden, V. Gokhale, V. D. Wheeler, A. R. Kramer, J. E. Yater, H. G. Xing, D. Jena, and D. J. Meyer, *Phys. Status Solidi A* **217**(3), 1900675 (2020).
- D. S. Katzer, N. Nepal, D. J. Meyer, B. P. Downey, V. D. Wheeler, D. F. Storm, and M. T. Hardy, *Appl. Phys. Express* **8**(8), 085501 (2015).
- M. A. Scarpulla, C. Gallinat, S. Mack, J. Speck, and A. Gossard, *J. Cryst. Growth* **311**(5), 1239–1244 (2009).
- C. Ziebert and S. Ulrich, *J. Vac. Sci. Technol., A* **24**(3), 554–583 (2006).
- R. Harrison and W. Lee, *Adv. Appl. Ceram.* **115**(5), 294–307 (2016).
- H. Bhuvaneshwari, K. Hembram, V. R. Reddy, and G. M. Rao, *Optoelectron. Adv. Mater.* **1**(6), 294–298 (2007).
- R. Potjan, M. Wislicenus, O. Ostien, R. Hoffmann, M. Lederer, A. Reck, J. Emará, L. Roy, B. Lilienthal-Uhlig, and J. Wosnitza, *Appl. Phys. Lett.* **123**(17), 172602 (2023).
- A. Cassinese, M. Iavarone, R. Vaglio, M. Grimsditch, and S. Uran, *Phys. Rev. B* **62**(21), 13915 (2000).
- M. H. Oliver, J. L. Schroeder, D. A. Ewoldt, I. H. Wildeson, V. Rawat, R. Colby, P. R. Cantwell, E. A. Stach, and T. D. Sands, *Appl. Phys. Lett.* **93**(2), 023109 (2008).
- S. Kalal, M. Gupta, and R. Rawat, *J. Alloys Compd.* **851**, 155925 (2021).
- D. S. Katzer, N. Nepal, M. T. Hardy, B. P. Downey, D. F. Storm, E. N. Jin, and D. J. Meyer, *J. Vac. Sci. Technol., B* **37**(3), 031211 (2019).
- B. J. May and R. C. Myers, *J. Vac. Sci. Technol., B: Nanotechnol. Microelectron.* **36**(1), 011203 (2018).
- M. Renninger, *Z. Phys.* **106**, 141–176 (1937).
- A. Jain, S. P. Ong, G. Hautier, W. Chen, W. D. Richards, S. Dacek, S. Cholia, D. Gunter, D. Skinner, G. Ceder, and K. A. Persson, *APL Mater.* **1**(1), 011002 (2013).
- B. O. Johansson, H. T. G. Hentzell, J. M. E. Harper, and J. J. Cuomo, *J. Mater. Res.* **1**(3), 442–451 (1986).
- H. M. Benia, M. Guemmaz, G. Schmerber, A. Mosser, and J. C. Parlebas, *Catal. Today* **89**(3), 307–312 (2004).
- S. Khan, M. Mehmood, I. Ahmad, F. Ali, and A. Shah, *Mater. Sci. Semicond. Process.* **30**, 486–493 (2015).
- K. Gofryk, M. Pan, C. Cantoni, B. Saporov, J. E. Mitchell, and A. S. Sefat, *Phys. Rev. Lett.* **112**(4), 047005 (2014).
- P. R. West, S. Ishii, G. V. Naik, N. K. Emani, V. M. Shalaev, and A. Boltasseva, *Laser Photonics Rev.* **4**(6), 795–808 (2010).
- G. V. Naik, V. M. Shalaev, and A. Boltasseva, *Adv. Mater.* **25**(24), 3264–3294 (2013).
- Q. Guo, T. Wang, Y. Ren, Y. Ran, C. Gao, H. Lu, Z. Jiang, and Z. Wang, *Phys. Rev. Mater.* **5**(6), 065201 (2021).